

ARTICLE OPEN



Marine heatwave as a supercharger for the strongest typhoon in the East China Sea

Iam-Fei Pun ¹✉, Huang-Hsiung Hsu ², Il-Ju Moon ³, I-I Lin ⁴ and Jin-Yong Jeong ⁵

Due to the cold water temperatures, the East China Sea (ECS) is usually unfavorable for typhoon development. Recently, in a rare event, Typhoon Bavi (2020) reached major typhoon status and became the strongest typhoon in the ECS in the past decade. Based on in situ observations and model simulations, we discover that this typhoon is fueled by a marine heatwave, which creates a very warm ocean condition with sea surface temperature (SST) exceeding 30 °C. Also, because of suppressed typhoon-induced SST cooling caused by the shallow water depth (41 m) and strong salinity stratification (river runoff) within the ECS, the SST beneath the typhoon remains relatively high and enhances the total heat flux for the typhoon. More interestingly, due to the fair weather ahead of the typhoon, we find that the rapid development of this marine heatwave is likely, in part, attributed to the typhoon itself. As the risks from typhoons and marine heatwaves are heightening under climate change, this study provides important insights into the interaction between typhoons and marine heatwaves.

npj Climate and Atmospheric Science (2023)6:128; <https://doi.org/10.1038/s41612-023-00449-5>

INTRODUCTION

In late August 2020, Typhoon Bavi unusually strengthened to Category 3 on the Saffir-Simpson wind scale when it was traveling up over the East China Sea (ECS) (Fig. 1), prompting North Korea to live broadcast the status of this typhoon and issue one of the first typhoon warnings in its history. Geographically, the ECS is a semi-closed marginal sea located in the northwest portion of the western North Pacific, where the water depth is generally <100 m. With a lifetime maximum intensity of 100 knots ($1 \text{ kt} \cong 0.51 \text{ m s}^{-1}$ or 1.85 km h^{-1}) attained at the southwest of Jeju Island, Typhoon Bavi was one of the two strongest typhoons ever occurred in this shallow water region. However, its intensity increase was the largest in the ECS region, with a total increase of 25 kt (from 75 to 100 kt) in about 1.5 days. In fact, an intense typhoon like this is extremely rare in the interior of the ECS, namely, at a latitude higher than 30°N. According to the 30 years of typhoon best track record¹ during 1991–2020, only 6.7% (32 out of 480) of the western North Pacific typhoons ended up in the ECS (Supplementary Fig. 1). Yet most of these typhoons reached their lifetime maximum intensity in the open western North Pacific Ocean, with 81.8% of them actually experiencing a decay over the ECS. Moreover, typhoons that achieved their lifetime maximum intensity, or what we may call here the “authentic” ECS typhoons, merely account for 1.3% (i.e., only six typhoons) of the total western North Pacific typhoons. This statistic truly reflects the fact that in this ECS region, the atmospheric and oceanic environments are both detrimental to typhoon development. Strong vertical wind shears and sharp ocean temperature gradients are common in the ECS^{2–6}. Climatologically, the bottom water temperature in this shallow basin can be as cold as 12 °C, which is due to the spread of cold water sinking from the northern Yellow Sea in winter time^{2,3}. During summer, however, the ECS is highly stratified by strong solar insolation, setting warm water on top and rather cold water at the bottom. Given this hydrographical condition, typhoons can easily generate excessive sea surface

temperature (SST) cooling, often up to 10 °C, in the ECS^{2–4,6}. It is well-known that typhoon-induced SST cooling is an essential negative feedback in typhoon intensification. It can effectively decrease the air-sea temperature disequilibrium and thus significantly reduce or even reverse the vital energy flux transferring from the ocean to the typhoon^{7–21}. Therefore, partially because of strong SST cooling, the majority of typhoons tend to decay in the ECS².

Recent studies found that the shallow bathymetry near continental coasts may play an essential role that may facilitate the intensification of landfalling typhoons^{22,23}. Induced by the gusty winds, the vertical mixing is usually the primary mechanism responsible for SST cooling beneath a typhoon^{7,11,13,15,16,23–29}. In general, the mixing depth (or length) of a typhoon, namely, the water depth at which the typhoon forcing can reach, varies from tens to 100 m or so, depending on ocean stratification and typhoon characteristics such as wind speed, moving rate and size^{4,13,16,21,25–27,30–32}. A deeper typhoon mixing depth will usually lead to stronger SST cooling since more cold water is being entrained upward to the sea surface. However, in shallow waters, regardless of how strong or slow the typhoon is or travels, the maximum mixing depth will be capped by natural bathymetry. For this reason, the typhoon-induced SST cooling would be significantly suppressed or even vanish in shallow waters, eventually boosting the typhoon intensity^{22,23}. However, the magnitude of SST cooling in shallow waters still largely depends on the temperature structure of the water column. As in the ECS and other continental shelf areas at similar latitudes, such as the Mid-Atlantic Bight on the west side of the North Atlantic Ocean, the pre-existing strong ocean stratification and cold bottom water often lead to profound SST cooling even though there is a depth limitation for vertical mixing^{33,34}.

However, this seemly unfavorable condition may be transformed by an extreme ocean warming event, such as a marine heatwave^{35–38}. Similar to an atmospheric heatwave, a marine

¹Graduate Institute of Hydrological and Oceanic Sciences, National Central University, Taoyuan, Taiwan. ²Research Center for Environmental Changes, Academia Sinica, Taipei, Taiwan. ³Typhoon Research Center, Jeju National University, Jeju, South Korea. ⁴Department of Atmospheric Sciences, National Taiwan University, Taipei, Taiwan. ⁵Korea Institute of Ocean Science and Technology, Busan, South Korea. email: ipun@ncu.edu.tw

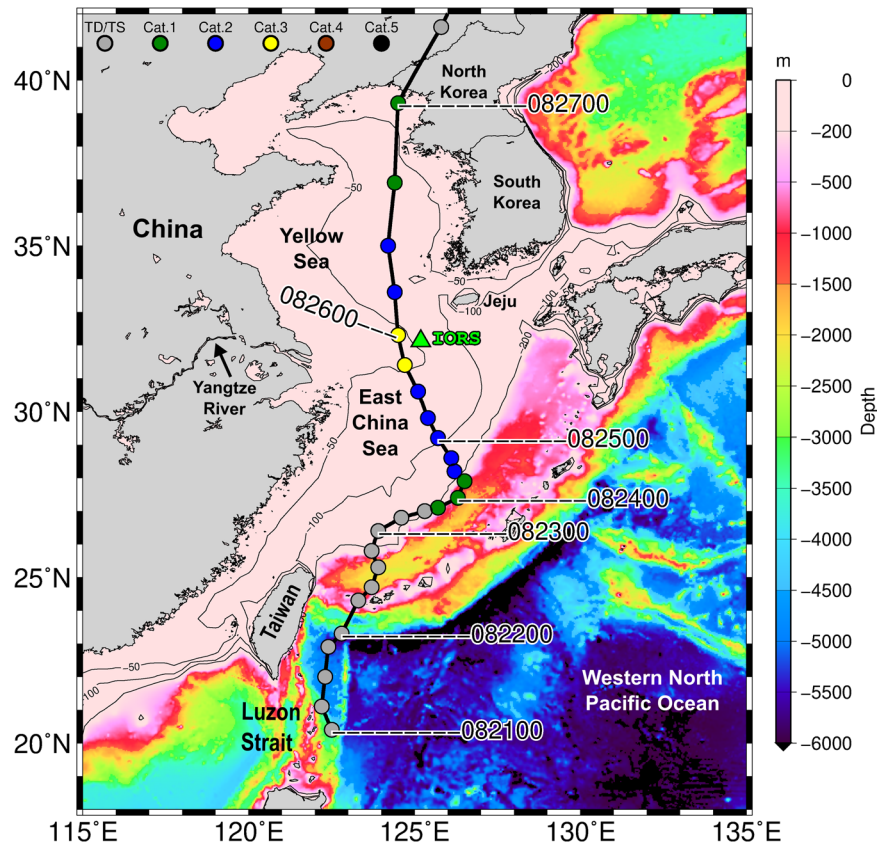


Fig. 1 Bathymetry of East Asia and track of Typhoon Bavi. The East China Sea and the Yellow Sea are marginal seas on the wide continental shelf with the water depth typically less than 100 m. Note that Typhoon Bavi passed the IORS site (depicted by the green triangle) with the peak intensity (100 kt) and made landfall on North Korea. The intervals of the track are 6 h with the time labels at each 0000 UTC. The colors of the typhoon dots indicate the Saffir-Simpson wind scale, which is shown in the upper-left corner. The bathymetry data is based on NOAA's 2-Minute Gridded Global Relief Data (ETOPO2).

heatwave is an extreme prolonged warming event occurring in the ocean, which can be caused by atmospheric and oceanic processes^{35–37}. A recent study conducted by Dzwonkowski et al.³⁹ pointed out that the ocean heat content in the coastal shallow water shelf in the northern Gulf of Mexico increased by twofold during the strike of a marine heatwave. They suggested that the doubled ocean heat content would likely enhance the intensity of the following hurricane that later made landfall on the US coast. In this study, we discovered that the ECS was experiencing a rapid warming just ahead of Typhoon Bavi, which is linked to a marine heatwave. Based on pairs of air-sea observations together with ocean mixed layer model simulations, we will show that the rapidly warmed shallow ECS effectively modulate the SST and total heat flux (i.e., the sum of sensible heat flux and latent heat flux) beneath Typhoon Bavi, allowing it to grow and become the strongest typhoon in this ECS region in the past decade.

RESULTS

SST condition in the ECS prior to Typhoon Bavi

Figure 2 shows SST analysis from cloud-penetrating satellite microwave observations. It is found that the SST in the interior of the ECS was very high, reaching 31 °C on 23 August when Typhoon Bavi was still at the south rim of the continental shelf (Fig. 2a). This is a huge contrast as compared to the long-term mean SST in August, which shows that the normal SST is around 28–29 °C (Fig. 2b). From the SST difference map (Fig. 2c), one can clearly see that a patch of positive SST anomaly as large as 3 °C appeared in the ECS, especially near its northern boundary where Typhoon Bavi archived and maintained its lifetime maximum

intensity. More interestingly, we also found that these high SST values were, in fact, a result of a rapid warming process taking place in the ECS. In early August 2020, the SST in the ECS was about 1 °C below the long-term mean, but somehow the SST started to increase sharply, totally increased by 4 °C in a short period (i.e., 9–23 August) until the arrival of the edge of Typhoon Bavi (Fig. 2d). This warm SST formed a perfect condition for the typhoon to intensify.

Notably, this abnormally high SST was linked to a marine heatwave event (see “Methods”) that struck the ECS area between 15 and 24 August 2020, just right before the passage of Typhoon Bavi. As revealed by the daily satellite SST maps (Fig. 3), this marine heatwave initially occurred in a confined area in the southern ECS on 15 August 2020. In the next 9 days, it quickly spread out almost the entire ECS and reached the maximum intensity of about 1.5 °C (above the 90th percentile level) between 21 and 24 August 2020 (Supplementary Fig. 2). This extreme ocean warming event reserved a large amount of heat energy awaiting the coming typhoon.

Air-sea measurements from the IORS

To improve monitoring and understanding of the air and sea environments and their associated interaction processes, South Korea has constructed three permanent, multifunctional research platforms in the ECS and Yellow Sea⁴⁰. On August 26, 2020, Typhoon Bavi closely passed by the southernmost station, i.e., the Ieodo Ocean Research Station (IORS), about 60 km to the left of the station and with a peak intensity of 100 kt (Fig. 1). The IORS is located at the boundary between the ECS and Yellow Sea, where

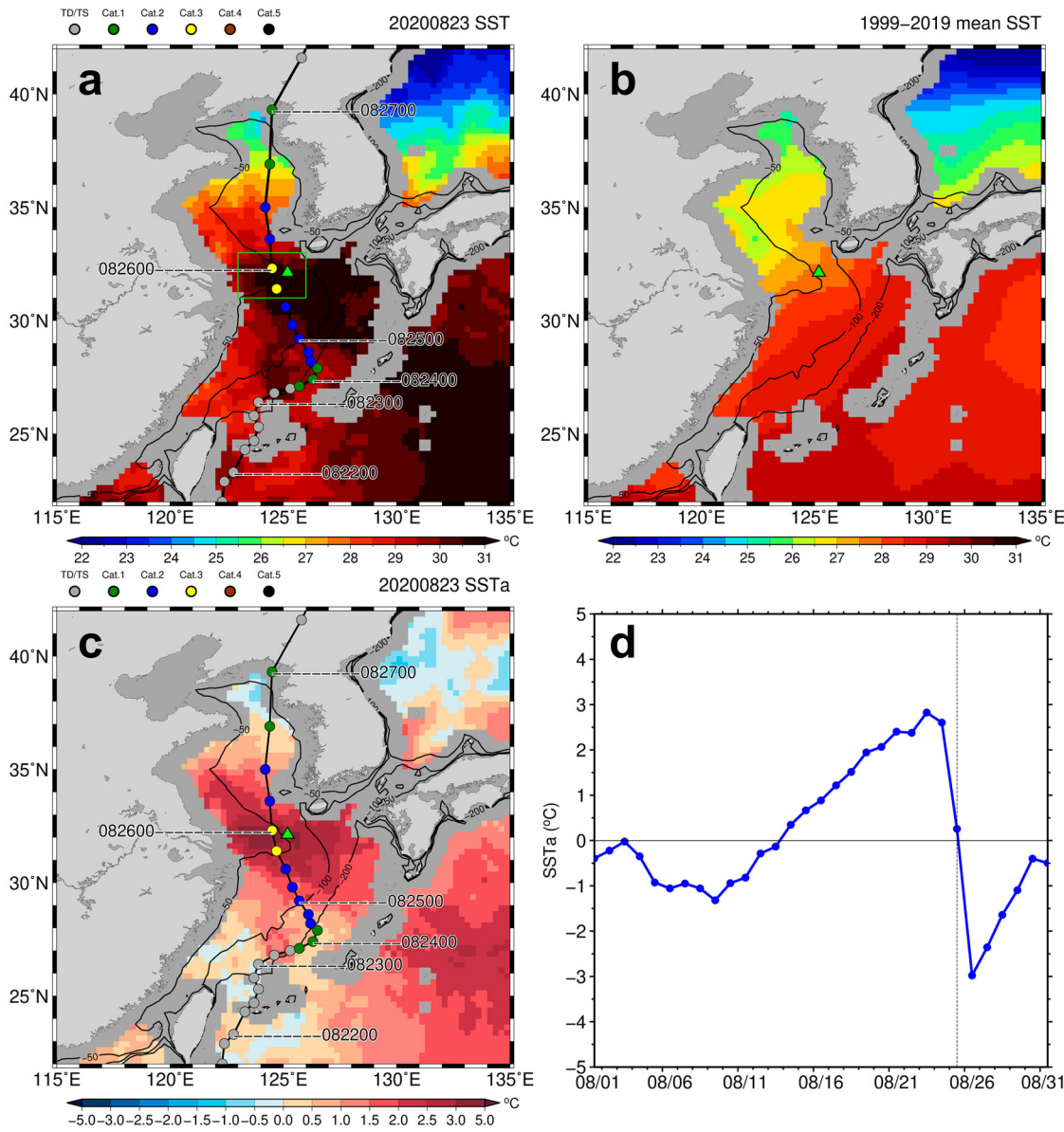


Fig. 2 SST analyses from cloud-penetrating satellite microwave observations. **a** SST map prior to the passage of Typhoon Bavi on August 23, 2020. **b** Long-term mean SST in August between 1999 and 2019. **c** SST anomaly on August 23, 2020 with respect to long-term mean in (b). **d** Time series of SST anomaly in August 2020, which is averaged within the green box shown in (a). Green triangle and contours in (a–c) indicate the location of the IORS site and shallow water depths, respectively, while the vertical dashed line in (d) depicts the arrival of the edge of Typhoon Bavi. Note that the SST used here is from the optimally interpolated SST (OISST) dataset provided by the Remote Sensing Systems.

the water depth is nominally less than 50 m. The encounter allowed the IORS to record crucial parameters between the air-sea interface simultaneously before, during, and after the typhoon, providing a chance to understand the impacts of a marine heatwave and shallow water depth on SST cooling and the corresponding surface heat flux supply to the typhoon.

The IORS recorded the highest wind speed of 45 m s^{-1} and the minimum sea-level pressure of 966 hPa during the visit of Typhoon Bavi (Fig. 4a). Prior to the typhoon, namely, before 1600 UTC 23 August, the wind speed at the IORS was quite weak, only about $1\text{--}3 \text{ m s}^{-1}$. Meanwhile, the near-surface air temperature (Ta) measurement showed a prominent diurnal fluctuation, with a mean value of $29\text{--}30^\circ\text{C}$ before the typhoon (Fig. 4b). As the core area of the typhoon moving in, the air temperature dropped to $\sim 25^\circ\text{C}$, but shortly after that it bounced back and remained relatively stable at around 26°C . The near-surface relative humidity (RH) during the passage was also observed.

I.-F. Pun et al.

For the oceanic part, the IORS provides temperature and salinity measurements at depths of 3, 20.5, and 38 m, roughly covering the whole shallow water column (i.e., 41 m) at this location. Therefore, a rather complete ocean response during the period of Typhoon Bavi was captured. The evolution of ocean temperatures at the IORS is shown in Fig. 4c. Here, we assume the 3 m temperature as SST. The maximum SST cooling of 9°C was observed, decreasing from 30.5°C to 21.5°C . Based on the subsurface temperature observations at 20.5 m and 38 m, it is found that the water column became well-mixed shortly, about 1.5 h after the impact of the typhoon (i.e., the closest point to the IORS), as indicated by the fusion of the temperatures at all depths. The immediately well-mixed water temperature was about 23.7°C occurring at 0010 UTC on 26 August (Fig. 4c). However, the well-mixed temperature continued to decrease and even re-stratified. It should be noted that there were no data at 20.5 m and 38 m about 6 h after the typhoon had passed, due to the damage of the

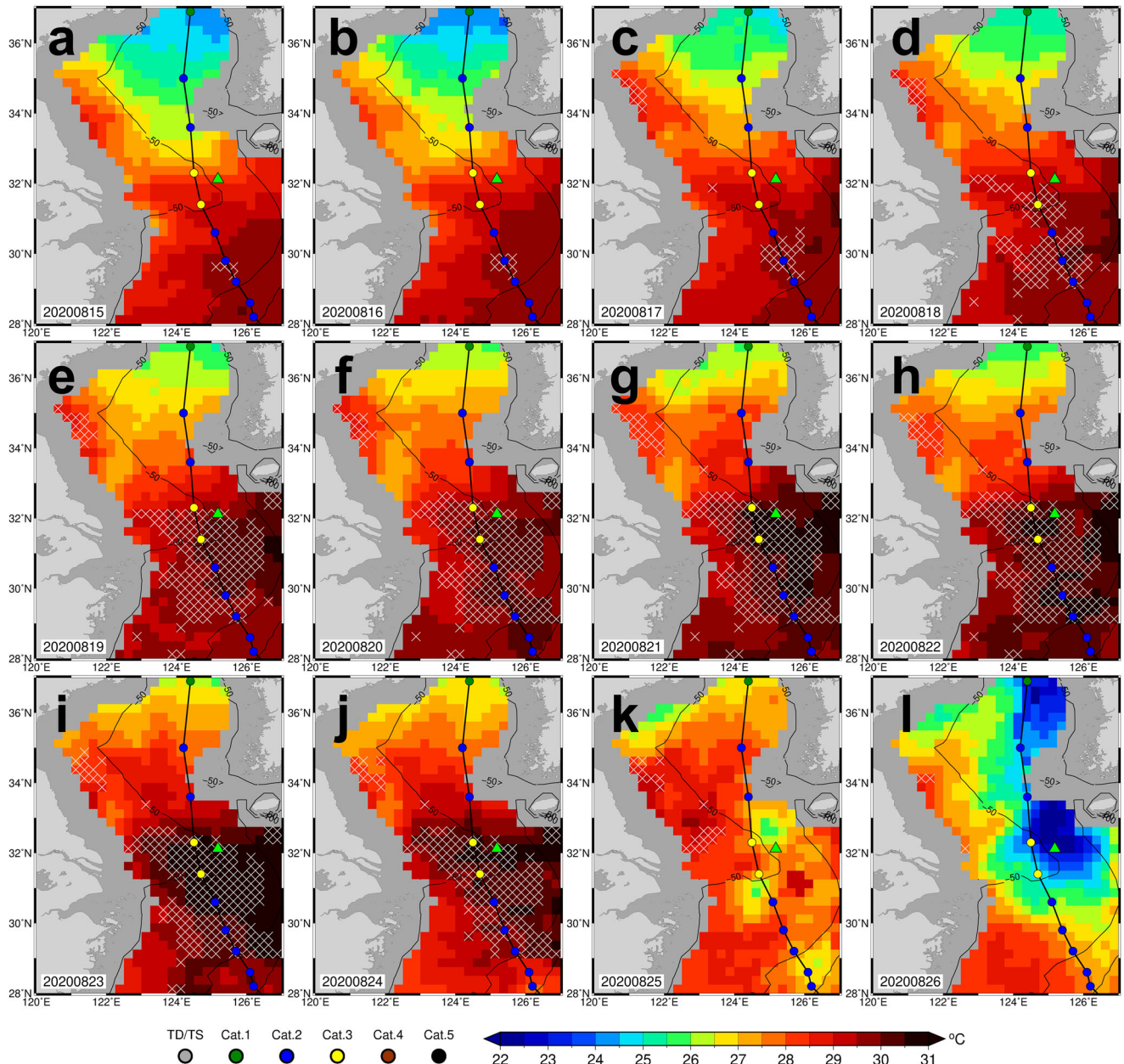


Fig. 3 Evolution of the marine heatwave. **a–l** A series of daily SST maps during the passage of Typhoon Bavi over the ECS from August 15 to August 26, 2020. The 0.25° grid points with white “x” symbol indicate the presence of marine heatwave. Green triangle and contours depict the location of the IORS site and shallow water depths, respectively. The time labels for the typhoon track can be found in Fig. 1.

sensors. In a typical situation, the water temperature is expected to be relatively steady when it was well-mixed^{23,26}. The continuous decrease of water temperature at the IORS could be caused by several factors. One possibility may be due to non-local effects, such as upwelling and lateral transports of water mass. Both may provide an additional source of cold water to cool off the water temperature. However, it is interesting to note that the maximum SST cooling occurred 7–8 h after the passage (i.e., at 0600 UTC 26 August), and then the temperature returned back to the initial well-mixed temperature and remained relatively stable afterward. At the IORS, the inertial period, i.e., $T = \frac{2\pi}{f}$ (with f being the Coriolis parameter), is ~ 22.6 h, therefore such fluctuation (i.e., from 2240 UTC 25 to 1400 UTC 26 August) is likely a result of the inertial oscillation. The temperature fluctuation ceased shortly may be due to the fact that larger ocean area was vertically well-mixed by the typhoon (Fig. 3l). According to these observations, we can

speculate that the water column at the IORS was more or less well-mixed right after the impact of Typhoon Bavi, and the well-mixed temperature was about 23.5 °C. In other words, if vertical mixing were the only physical mechanism for SST cooling, the maximum SST cooling in this water would be about 7 °C, due to the restriction of the shallow water depth.

The effect of the marine heatwave on SST cooling

Figure 5a shows the result of the marine heatwave experiment (MHW; see Methods). In general, the SST evaluation simulated by the Price-Waller-Pinkel (PWP) ocean model is in good agreement with the 3 m temperature at the IORS, except that the cooling evolved a little faster than the observation by about 2 h and that the cooling was underestimated after the well-mixed between 0100 UTC and 1400 UTC 26 August (dashed curve in Fig. 5a). The

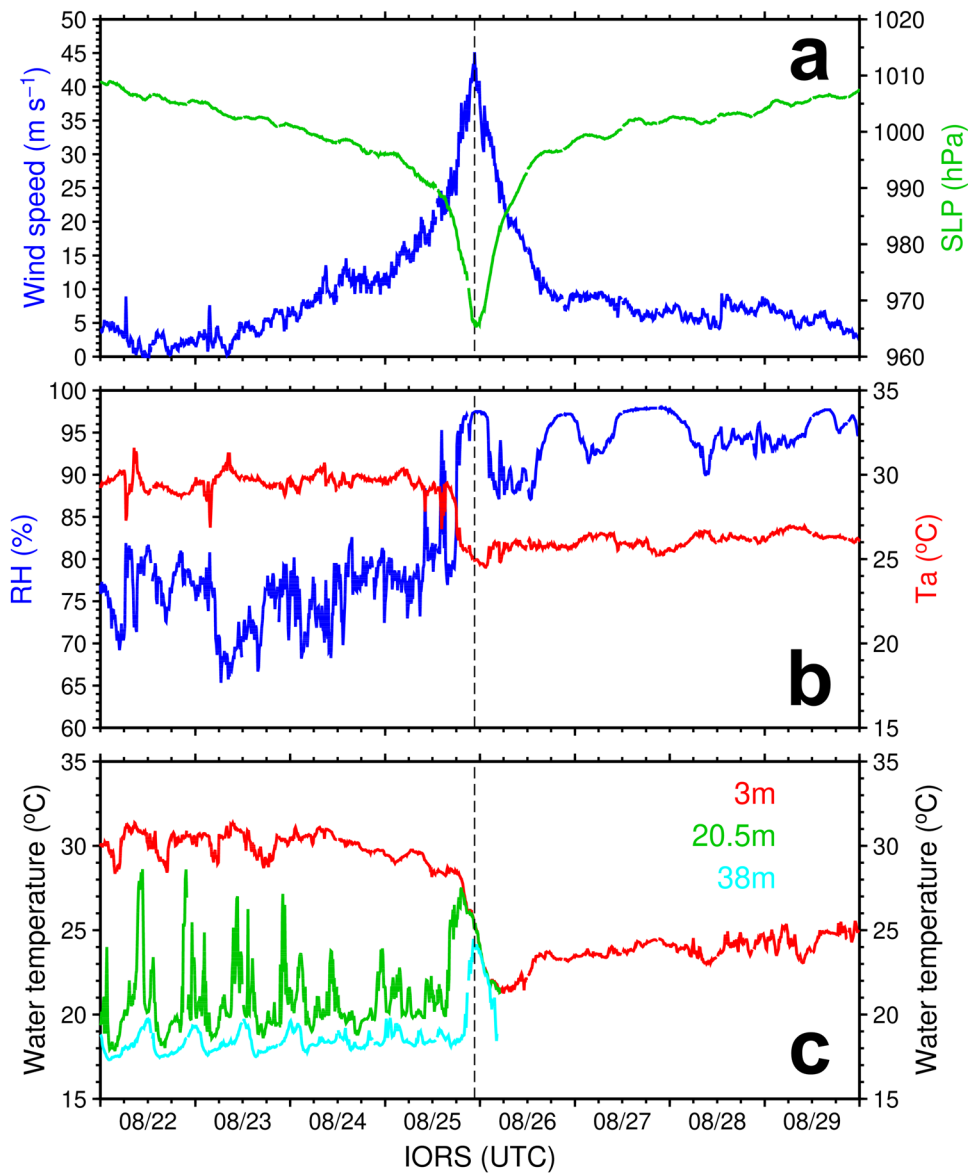


Fig. 4 Air-sea measurements from the IORS. **a** Wind speed and sea-level pressure (SLP). **b** Relative humidity (RH) and air temperature (Ta). **c** Ocean temperatures at depths of 3, 20.5, and 38 m. The location of the IORS is shown in Fig. 1.

final well-mixed temperature was 23.2 °C, which is very close to the IORS observation. In addition, the cooling rate is fairly consistent with the observation. It can be seen clearly when the model result is shifted forward by 2 h (red curve in Fig. 5a). This small time bias could be caused by background flows or horizontal advection of warm water which are not included in this simple PWP model. From the observation, it can be seen that the SST increased by 0.8 °C and 0.4 °C at around 0700 and 1700 UTC 25 August, respectively, before the rapid decrease. Such fluctuations may also delay the SST cooling. Nevertheless, this comparison indicates the good performance and reliability of the PWP in simulating the ocean response to a typhoon in which vertical mixing dominates. Since the time bias seems systematic, we calibrated all the PWP results by shifting 2 h forward.

Figure 5b shows the results of SST cooling simulated by the PWP model. Here, the SST cooling is defined as a positive value with respect to the initial SST. The deviation from the MHW experiment indicates the influence of the factor tested in the corresponding experiment. By comparison, it is found that the experiment without the marine heatwave situation (i.e., No_MHW)

produced the least SST cooling. The total SST cooling in the No_MHW experiment was 5.1 °C, which is 1.9 °C less than the MHW experiment (Table 1). It suggests that the SST cooling is even smaller without the presence of the marine heatwave. The reason for this outcome is that in our assumption only the near-surface layer was affected by the marine heatwave (Supplementary Fig. 3b). In such situation, colder initial SST associated with the No_MHW experiment actually reduces the ocean temperature gradient and hence leads to a somewhat counterintuitively weaker SST cooling. The effect of uneven warming within the water column on SST cooling has been pointed out by previous studies^{41,42}. However, it is important to note that smaller SST cooling does not necessarily mean warmer SST underneath the typhoon (i.e., during-typhoon SST = initial SST – SST cooling induced by the typhoon). In fact, since the initial SST was several degrees colder in no marine heatwave situation (i.e., 2.9 °C colder as compared to the MHW experiment), the during-typhoon SST simulated in the No_MHW experiment turned out to be much lower (Fig. 5c and Table 1), even though it had the least SST cooling. This result will have a strong implication for air-sea heat

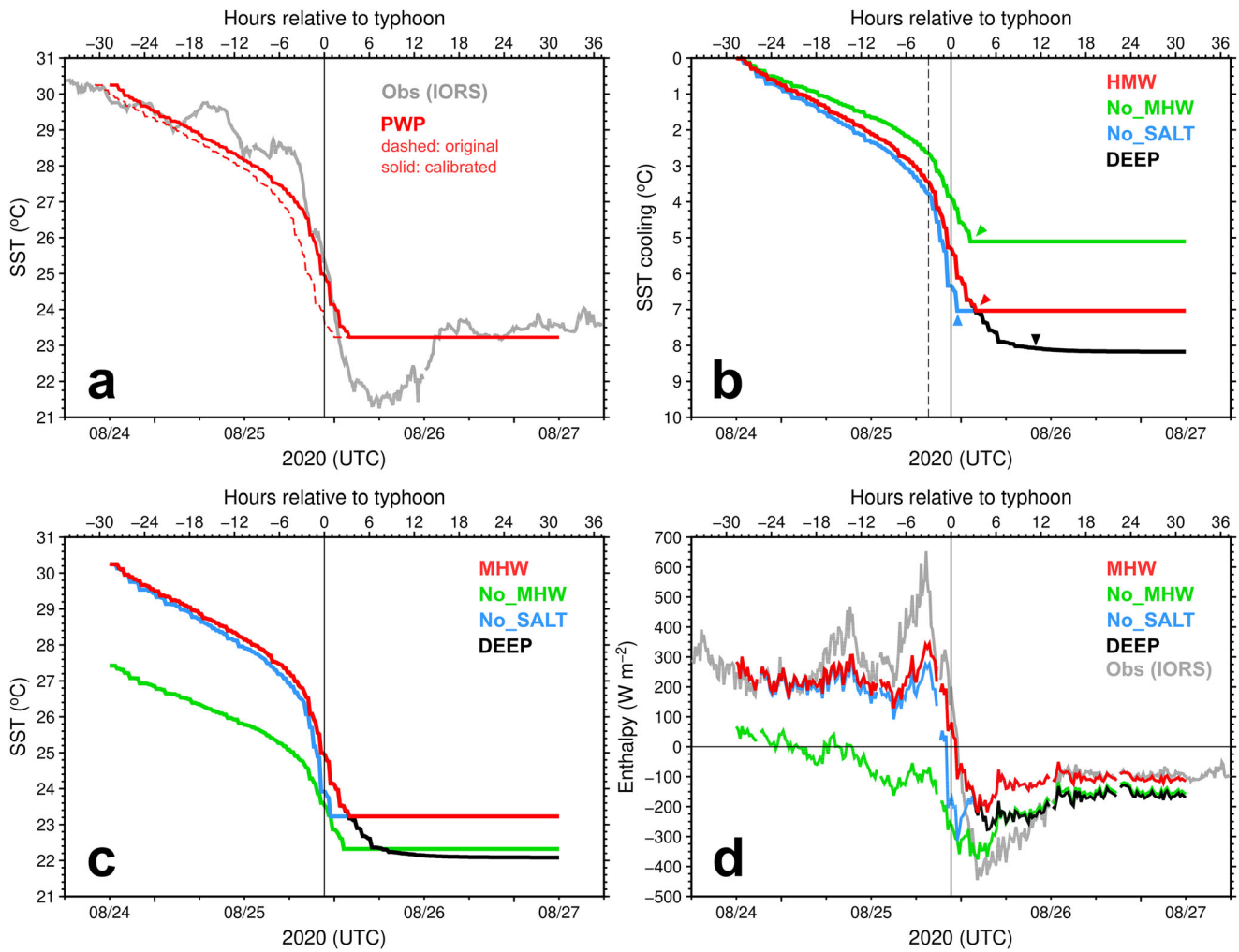


Fig. 5 Results of PWP simulations. **a** SST comparisons between IORS observation (gray) and PWP model simulations, in which the red dashed curve represents the original output of the MHW experiment, while the red solid curve represents the same output but with calibration of 2 h. **b** SST cooling results for the four PWP experiments. The vertical dashed line depicts 3 h before the impact of the typhoon, while the arrowheads indicate the time of well-mixed in different experiments. **c** Same as (b), but for absolute SST. **d** Same as (b), but for total heat fluxes. The color codes are shown in each plot and the vertical line indicates the impact of the typhoon. The upper axis shows the hours relative to the typhoon.

fluxes. In addition to the magnitude of SST cooling, owing to weaker stratification, the well-mixed temperature was achieved 0.75 h faster.

Effect of the marine heatwave on SST and heat fluxes

Although SST cooling is deemed to be a critical indicator in terms of the energy exchange at the air-sea interface, the amount of energy transferred depends on the absolute SST value underneath the typhoon^{43,44}. Therefore, it is necessary to examine the during-typhoon SST in order to understand the heat transferred between the ocean and the typhoon. Figure 5c shows the SST evolutions in the PWP experiments. As mentioned above, the marine heatwave had an overwhelming effect on the absolute SST value, despite there was more SST cooling. Without the marine heatwave, the SST would be much colder over the entire period (green curve vs. red curve in Fig. 5c). For example, the SST would be 1.5 °C and 0.9 °C lower underneath the typhoon and after the well-mixed, respectively (Table 1). It is important to note that this small SST difference under the typhoon was large enough to change the direction of energy transfer. As shown in Fig. 5d, with the marine heatwave as in the MHW experiment, the total heat flux was able to maintain positive (+76 W m⁻²) at the time Typhoon Bavi was

passing through the IORS, meaning that the typhoon was still receiving energy from the ocean. However, if it were a normal condition, i.e., without the presence of the marine heatwave as in the No_MHW experiment, the total heat flux would become a large negative value (-259 W m^{-2}) (Table 1). In fact, the total heat flux would be already nearly zero even before the typhoon stirring up the ocean (green curve in Fig. 5d). In such condition, Typhoon Bavi would have no way to sustain its intensity in the ECS. It is also noteworthy that the total heat flux estimated from the MHW experiment generally agrees with the observation at the IORS (red and gray curves in Fig. 5d). From the observation, we can see that the ocean continuously transferred energy to the atmosphere until the impact of Typhoon Bavi. But quickly, the total heat flux dropped sharply and turned into negative, meaning the reverse of energy directed from the atmosphere to the ocean.

The roles of shallow water depth and salinity stratification

According to the no ocean bottom experiment (i.e., DEEP), it is found that the shallow water depth started to take effect about 3 h after the impact of Typhoon Bavi. Before that, it had no effect on SST cooling. Without the bottom depth constraint, the SST cooling would continue to grow until the surface forcing relaxed.

Table 1. SST, SST cooling, and total heat flux.

	Before (-29 h)	During (0 h)	After (18 h)
SST (°C)			
MHW	30.3	25.0	23.2
No_MHW	27.4	23.5	22.3
No_SALT	30.3	23.9	23.2
DEEP	30.3	25.0	22.1
SST cooling (°C)			
MHW	-	5.3	7.0
No_MHW	-	3.9	5.1
No_SALT	-	6.3	7.0
DEEP	-	5.3	8.2
Total heat flux (W m^{-2})			
MHW	283	76	-107
No_MHW	67	-259	-157
No_SALT	283	-173	-107
DEEP	283	76	-169

These values are from the PWP simulations at the IORS at different stages relative to the impact of Typhoon Bavi. Their full-time evolutions are shown in Fig. 5b–d.

As we can see from the black curve in Fig. 5b, the SST cooling became relatively stable about 8 h after the typhoon's passage. The final SST cooling was 8.2 °C in this experiment, which is 1.2 °C or 17% stronger than the actual condition with depth limitation (Table 1). This result indicates that the presence of shallow water depth has a strong suppression effect on SST cooling, though in this case most of its contribution was a little after the impact of the typhoon. Similarly, without the bottom boundary the SST would continue to drop to 22.1 °C (black curve in Fig. 5c). And owing to the colder SST, the total heat flux for the second half of the passage (i.e., from about 3 h after the impact of the typhoon) would become more negative, from about -107 W m^{-2} in the situation with the actual water depth to about -169 W m^{-2} with no bottom depth (Fig. 5d and Table 1). This accounts for a 58% difference. It is interesting to note that this part of the heat flux is corresponding to the rear half of the typhoon as it moving away from the IORS. The enhanced negative flux (losing energy to the ocean) would likely affect the subsequent decay rate and landfall intensity as Typhoon Bavi crossed the Yellow Sea on a northerly track.

Since the background salinity structure at the IORS site is usually predominated by the runoff from one of the world's largest river systems⁴⁵, i.e., the Yangtze River, the large amount of freshwater enhances the stratification of the water column and creates a barrier layer that could significantly resist the vertical mixing⁴⁶ (Supplementary Figs. 4 and 5). Therefore, if the salinity-related stratification was removed as in the constant salinity experiment (i.e., No_SALT), we can see that the SST cooling immediately became more drastic and evolved at a faster pace, especially under the high wind regime (blue curve in Fig. 5b). The cooling rates with and without salinity effect can have a 1.5-fold difference (i.e., 0.57 °C per hour vs. 0.86 °C per hour). Note that the cooling rate was computed over the period from 3 h before the impact of the typhoon to the time the water column became well-mixed. Because of that, beneath typhoon SST cooling was 1.0 °C or 19% stronger as compared to the salinity-stratified situation (i.e., the MHW experiment) (Table 1). In other words, the salinity-induced stratification can significantly restrain the SST cooling inside the typhoon's core area. However, we can see that the well-mixed (or terminal) temperature literally remained unchanged. This implies that no matter how strong the stratification is, it would more likely

be broken by the intense typhoon forcing sooner or later. Nevertheless, from the typhoon perspective, what really matters is the SST underneath, and the salinity here seems to play a role in this case.

In the situation without salinity stratification, the during-typhoon SST was much colder due to stronger SST cooling (blue curves in Fig. 5b, c). As a result, there was a significant reduction in the total heat flux, especially right under the typhoon, it would become a negative value of -173 W m^{-2} (Fig. 5d and Table 1). This means that the typhoon would be losing energy to the ocean in the IORS area if there were no salinity stratification to resist vertical mixing. However, the salinity effect quickly vanished, in about 3 h after the impact of the typhoon when the water column became well-mixed. After that, the salinity had no effect on the SST and total heat flux (Fig. 5c, d and Table 1).

Figure 6 illustrates the total heat flux at the IORS with the relative typhoon positions from 1200 UTC 25 August to 0600 UTC 26 August. From the observation (Fig. 6a–d), it is clear that the front half of the typhoon continuously received increasing heat flux, ranging from $+246$ to $+471 \text{ W m}^{-2}$ as the typhoon approaching the IORS. The positive fluxes partially explain the reason why Typhoon Bavi was able to maintain the Category-3 intensity in this ocean basin where is used to be unfavorable for typhoon development. Right after the passing of the typhoon center, the total heat flux immediately flipped into negative, falling from -89 to -335 W m^{-2} . This indicates that the rear half of the typhoon was actually losing energy to the ocean. The changing sign of the flux is consistent with the fact that Typhoon Bavi started to weaken after passing the IORS.

Based on our simulations, the marine heatwave had a manifest contribution to the total heat flux. Without the extreme warming from the marine heatwave, Typhoon Bavi would not have had a chance to obtain energy from this ocean basin, as we can see that the heat fluxes were all negative over the entire passing (Fig. 6e–h). This implies that Typhoon Bavi would not be able to develop into the strongest typhoon in this ECS region without the aid of the marine heatwave.

The effect of salinity stratification tends to concentrate in a relatively short period within the typhoon center. The strong salinity stratification ensures additional heat flux transferring to the typhoon, thus likely to maintain the typhoon intensity around the IORS region. Otherwise, the heat flux would be too small and even negative to support a Category-3 strength typhoon (Fig. 6i–l). For the shallow water depth, we can see that it has a considerable modulation on the heat flux in the northern ECS, but mainly for the rear half of the typhoon (Fig. 6m–p). The shallow water depth significantly limits the growth of the negative heat flux, due to its suppression effect on the SST cooling. It is believed that the restriction on negative heat flux may slow down the decay rate of the typhoon and hence enhance the landfall intensity and the risk of the typhoon.

DISCUSSION

From the air-sea energy aspect, we have demonstrated the dominant role of the marine heatwave in the extraordinary intensity that Typhoon Bavi achieved in this marginal sea. An increasing number of studies have shown that atmospheric heatwaves will become more frequent and last longer under the influence of climate change^{47–50}. How its oceanic counterpart behaves is one of the most imperative problems in marine ecosystems and should have a far-reaching implication on typhoon activity and intensification^{51,52}. Coastal marine heatwaves, such as the one experienced by Typhoon Bavi, are of particular importance because they may mount extra risk and uncertainty on landfalling typhoons. As mentioned above, the SST over the interior of the ECS warmed so fast that exceeded the threshold of the marine heatwave definition just a few days before

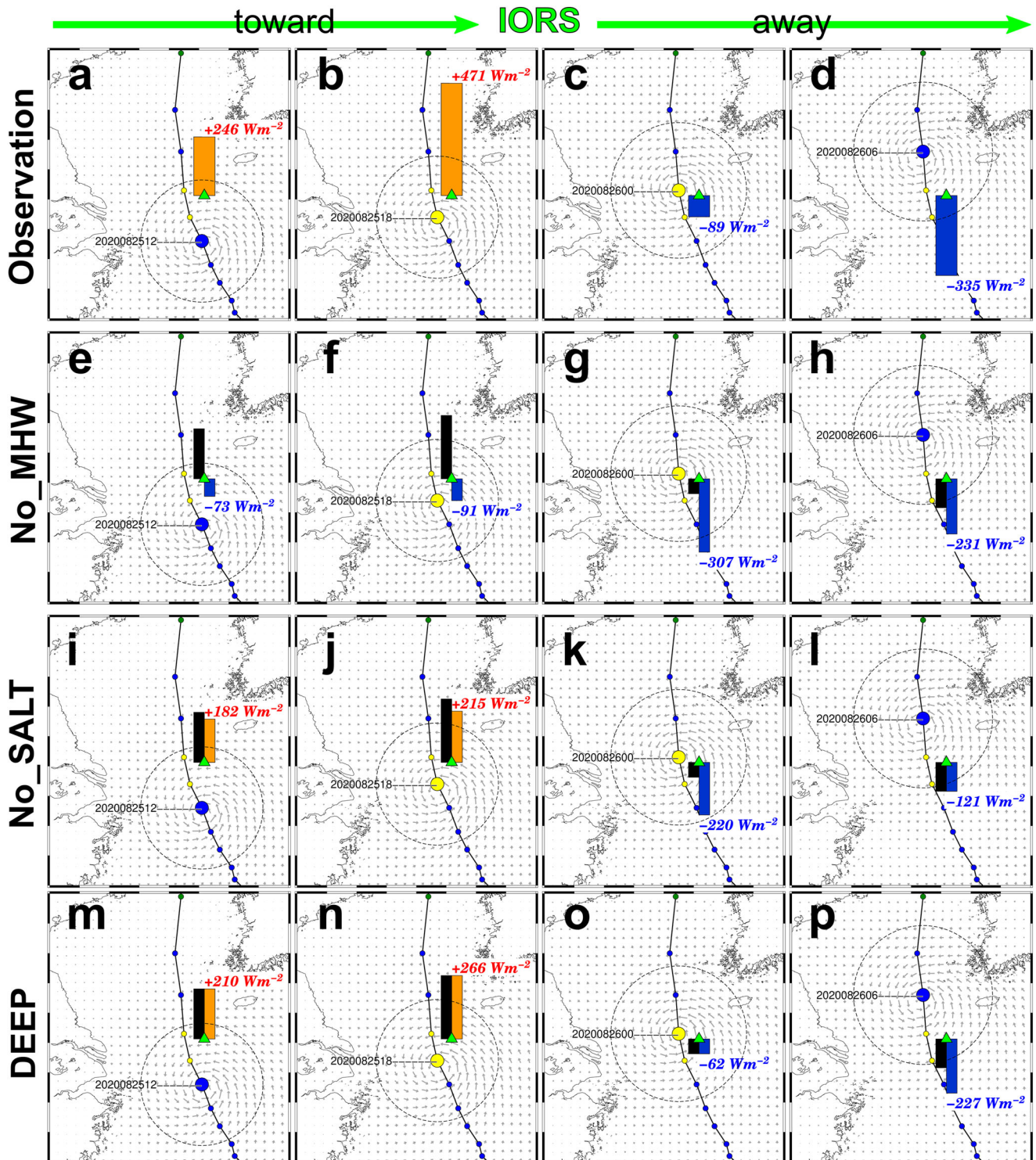


Fig. 6 Total heat fluxes at IORS during the passage of Typhoon Bavi. **a–d** Computed from IORS air-sea parameters; **e–h** from the No_MHW experiment; **i–l** from the No_SALT experiment; and **m–p** from the DEEP experiment. The length of vertical bars is proportional to the total heat flux with the zero value centered at the IORS location (green triangle). The corresponding flux values are also indicated. For comparison, the black vertical bars show the values from the MHW experiment. The first two columns of plots represent the situation when the typhoon is approaching to the IORS, while the last two columns are away.

the typhoon's passage (Fig. 3 and Supplementary Fig. 2). We found that this rapid SST warming may be attributable to the typhoon itself. Away from typhoon convective zones it is usually dominated by subsiding airflows, which leads to fair-weather conditions accompanied by a high-pressure system. The

adiabatically warmed air and excessive solar insolation uninterrupted illuminate the ocean surface and eventually trigger a rapid SST warming. A recent study by Lok et al.⁵³ indicated that such ahead-of-typhoon radiative forcing indeed increased the coastal water temperature and hence, may alter typhoon's landfall

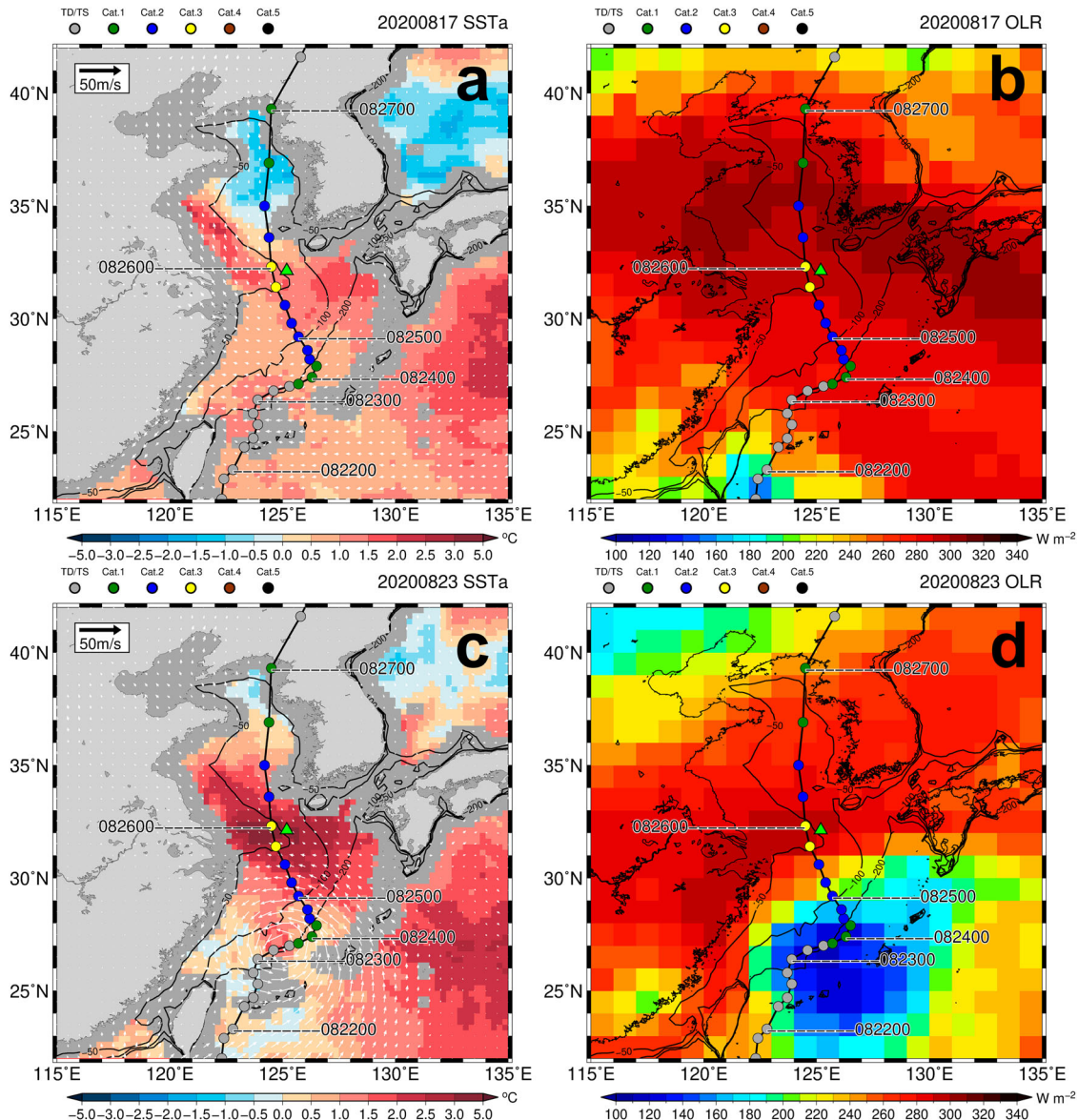


Fig. 7 Ocean surface winds and outgoing longwave radiation prior to Typhoon Bavi. **a** Ocean surface winds (vectors) and SST anomaly with respect to long-term mean of August (shading) on August 17, 2020. **b** Outgoing longwave radiation on August 17, 2020. **c, d** Same as **(a, b)**, but for August 23, 2020. The ocean surface winds and SST anomaly are based on the Cross-Calibrated Multi-Platform version 2 (CCMPv2) and OISST products from the Remote Sensing Systems. The outgoing longwave radiation data are from Climate Data Record distributed by NOAA.

intensity. To verify the potential connection between the typhoon and marine heatwave, we further inspected ocean surface wind and outgoing longwave radiation (OLR) prior to the typhoon. It is found that a large area of the ECS and Yellow Sea was under a clear sky with wind speed of 5 m s^{-1} or less (Fig. 7). This weather condition enabled the ocean surface to absorb more downward radiative energy and also reduce the heat flux losing to the air. As the typhoon approaching, the surface winds over the ECS and Yellow Sea were further suppressed by the downdraft. As a result, the effects of latent and sensible heat fluxes strengthened and the SST increased even more dramatically, and finally, the marine heatwave was established. This finding suggests that this marine heatwave event was likely in part attributed to the typhoon itself in advance. After that, the overheated ocean served as a huge energy reservoir feeding back to the passing typhoon by enhancing the air-sea heat flux.

So far, the marine heatwave refers solely to a phenomenon associated with extreme SST values. How much warming below

the sea surface is crucial regarding SST cooling and air-sea heat fluxes underneath the typhoon. If the marine heatwave-led extreme warming is only confined within the very surface of several meters, its impact on typhoons would be limited because such warming will be quickly diluted by the strong wind mixing. In this study, although the leodo Ocean Research Station, i.e., IORS, has provided valuable in situ observations delineating the vertical temperature structure in this shallow water area, it is not enough to fully resolve the effect of the marine heatwave on the whole water column (c.f. Supplementary Fig. 3). Given the shallow water depth, any small changes in this thermal structure may easily alter the total SST response to the typhoon. Therefore, a more detailed thermal structure is desired in the future in order to further understand the vertical evolution of a marine heatwave and its influence on typhoon intensity change. Yet, this work only focused on the warming in the upper portion of the water column; how the temperature changed in the lower part is also important to

evaluate the contribution of the marine heatwave to this typhoon case.

In addition, coastal ocean dynamics can be very complex, with a wide range of interactions between tides, waves, currents, and physical boundaries^{2,33,54}. In this study, we simplified the problem into wind-driven vertical mixing. This assumption is supported by the IORS in situ observations, which illustrate that the SST cooling at the forced stage of Typhoon Bavi was primarily caused by vertical mixing. The good agreement between PWP simulations and IORS observations further confirms this point. However, there are still some missing parts, such as the short period of decreasing water temperature after the well-mixed of the water column (Fig. 4c). It is suggested that other processes, such as cold water advection, may come to play.

To summarize, we found that the marine heatwave, shallow water depth, and salinity stratification all collectively contribute to this unusual typhoon event in the ECS (Fig. 5d). In particular, the marine heatwave appears to be the main driver, which is responsible for a large amount of extra heat flux that Typhoon Bavi would never receive in a normal condition. These linkages and their individual contributions to the ocean response and the typhoon intensity change merit to examine further in the future with the aid of fully coupled typhoon-ocean models.

Lastly, the coasts around the ECS and Yellow Sea are home to over a half billion people. Any changes in typhoon activity in this marginal sea will have serious consequences for livelihood and even the global economy. With the looming of climate change, more extreme weather events such as atmospheric and marine heatwaves have occurred all around the world. Therefore, continuously monitoring the air and sea states with a higher resolution strategy, especially in the subsurface, is critical to improve typhoon forecasting and mitigate the impact of typhoons.

METHODS

Marine heatwave

We follow the procedure of ref. ³⁶ to define marine heatwaves. By definition, a marine heatwave represents the local SST that exceeds the 90th percentile of the daily SST values at the same location within the past 30 years, i.e., the so-called climatic period, and this exceedance SST must persist for at least 5 consecutive days. In this study, since the satellite microwave SST data are preferable and only available from 1998, we used 1998–2021, a total of 24 years, as a baseline to calculate marine heatwave. Note that the results are similar to the ones using the NOAA optimal interpolation SST dataset (<https://www.ncei.noaa.gov/products/optimum-interpolation-sst>), which contains a complete 30 years of data (not shown).

Model simulations

In this study, we conduct a series of numerical experiments using the Price-Weller-Pinkel (PWP) ocean mixing model to demonstrate the effects of the marine heatwave, shallow water depth, and salinity stratification on typhoon-induced SST cooling. Based on the IORS observations, the SST cooling induced by Typhoon Bavi in the northern ECS was mainly attributed to the local vertical mixing. For this reason and to reduce the complexity of the problem, the one-dimensional PWP model²⁷ (hereafter PWP) was employed. The PWP is a layer model driven by surface forcing. It has been widely used to study the ocean response to typhoons (e.g., ref. ²⁸). In the PWP, the vertical mixing between two adjacent oceanic layers is determined by three conditions, that is, the density-driven static instability, mixed layer instability due to wind drag current in the mixed layer, and shear instability induced by the currents below the mixed layer^{25,27,31}. The static instability is dominated by surface buoyancy fluxes, i.e., heat flux and

freshwater flux, since temperature and salinity are the main factors for seawater density. Vertical mixing occurs whenever the upper layer is denser than the lower layer, i.e.,

$$\frac{\partial \rho}{\partial z} < 0 \quad (1)$$

where ρ is seawater density and z is ocean depth. The momentum of the typhoon is transferred to the ocean via the wind stress (τ) and drives the current in the mixed layer. For calculating the wind stress, the drag coefficient (C_d) suitable for higher wind speed from ref. ⁵⁵ was used. The wind-driven current induces instability at the base of the mixed layer and leads to mixing (or so-called entrainment) with the layer just below. This instability is the primary mechanism responsible for mixed layer deepening, and is determined by the bulk Richardson number (R_b) in the PWP. That is,

$$R_b = \frac{g \Delta \rho h}{\rho_0 (\Delta V)^2} \quad (2)$$

where g is the acceleration due to gravity, h is the mixed layer thickness, ρ_0 is the reference seawater density taken as 1024 kg m^{-3} , and $\Delta \rho$ and ΔV are the density and current velocity differences between the mixed layer and the layer below, respectively. When the bulk Richardson number is lower than 0.65, it means that the mixed layer current is strong enough to trigger vertical mixing. Lastly, mixing between the layers below the mixed layer (i.e., h) is subject to the shear instability, which is represented by the gradient Richardson number:

$$R_g = \frac{g \partial \rho / \partial z}{\rho_0 (\partial V / \partial z)^2} \quad (3)$$

The mixing between two adjacent depths occurs when R_g is lower than 0.25. At each time step, the PWP will iterate and mix the temperature and salinity profiles until the whole water column becomes stable, according to the three instability criteria.

In this study, four PWP experiments, including one control experiment and three tested experiments, were carried out to examine the effects of a marine heatwave, shallow water depth, and salinity on the ocean response to the typhoon. All of the simulations ran from 1600 UTC 24 to 0400 UTC 27 August, a total of 2.5 days, covering the duration of Typhoon Bavi at the IORS. The surface wind forcing was directly from the IORS observations (Fig. 4a). The vertical resolution and time step of the model were set to 1 m and 15 min, respectively. Supplementary Fig. 3 shows the initial temperature and salinity profiles for the four simulations. The initial profiles for the marine heatwave experiment (MHW, or the so-called control experiment) were obtained by averaging the IORS observations between 1600 UTC 21 and 1600 UTC 23 August (Supplementary Fig. 3a), representing a pre-typhoon observed ocean condition. To examine the impact of the extreme ocean warming effect due to the marine heatwave, the first tested experiment was to substitute the temperature profile with the one re-constructed by the long-term mean SST of August (i.e., 27.4°C), representing a situation without the marine heatwave (i.e., No_MHW experiment; Supplementary Fig. 3b). The second experiment was devoted to test the salinity effect. To do that, the salinity was set to be homogeneous with a constant value of 35 psu, which is the vertical mean of the observed pre-typhoon salinity profile and represents no salinity-stratified situation (i.e., No_SALT experiment; Supplementary Fig. 3c). The last experiment was to test the constraint effect of the shallow water depth (i.e., DEEP experiment). In this experiment, the ocean depth was infinitely deep. The initial temperature beyond the IORS water depth was extrapolated according to the temperature gradient between 20.5 m and 38 m, while for the salinity it was set to the same value as at 38 m (Supplementary Fig. 3d). The contribution of each factor (i.e., marine heatwave, salinity

stratification, and water depth) on the SST cooling was evaluated by comparing with the result from the MHW experiment.

Air-sea heat fluxes

To calculate the sensible heat flux (Q_S) and latent heat flux (Q_L), we employed the bulk aerodynamic formulas^{8,12,33}:

$$Q_S = C_h W(T_s - T_a) \rho_a C_{pa} \quad (4)$$

$$Q_L = C_e W(q_s - q_a) \rho_a L_{va} \quad (5)$$

where W is the surface wind speed, ρ_a is the density of air taken as 1.2 kg m^{-3} , C_h and C_e are the exchange coefficients for sensible and latent heat, both taken as 1.3×10^{-3} based on measurements under high wind condition⁵⁶, T_s and T_a are the SST and near-surface air temperature, q_s and q_a are the surface and near-surface air specific humidity computed from T_s , T_a and relative humidity (RH), and C_{pa} and L_{va} are the air heat capacity and latent heat of vaporization, respectively. In this calculation, W , T_a , and RH are directly obtained from the IORS observations, whereas T_s can be based on observation or PWP simulations.

DATA AVAILABILITY

The Ieodo Ocean Research Station (IORS) observational data used in this study are provided by Korea Institute of Ocean Science and Technology, Republic of Korea. The temporal resolution of this dataset is 10 min. Typhoon best track data are from the Joint Typhoon Warning Center (JTWC; <https://www.metoc.navy.mil/jtvc/jtvc.html?best-tracks>). The $0.25^\circ \times 0.25^\circ$ daily SST, Sea Surface Salinity (SSS), and wind vector analysis are based on the optimally interpolated SST product (OISST), Soil Moisture Active Passive (SMAP) SSS V5.0 product, and Cross-Calibrated Multi-Platform (CCMP) Version 2.1 product, respectively, which are distributed by the Remote Sensing Systems (RSS; <https://www.remss.com/>). The bathymetry data is based on NOAA's 2-Minute Gridded Global Relief Data (ETOPO2; <https://www.ngdc.noaa.gov/mgg/global/relief/ETOPO2/ETOPO2v2-2006/>). The $1^\circ \times 1^\circ$ daily outgoing longwave radiation (OLR) data are from Climate Data Record distributed by NOAA (<https://www.ndbc.noaa.gov/products/climate-data-records/outgoing-longwave-radiation-daily>). The $0.25^\circ \times 0.25^\circ$ daily ECMWF's Ocean Reanalysis System 5 (ORAS5) data are from the Copernicus Marine Environment Monitoring Service (CMEMS; <https://doi.org/10.48670/moi-00024>).

CODE AVAILABILITY

The codes used in this study are available from the corresponding author on request.

Received: 18 April 2023; Accepted: 7 August 2023;

Published online: 28 August 2023

REFERENCES

- Chu, J. H., Sampson, C., Levine, A. S. & Fukada, E. The Joint Typhoon Warning Center Tropical Cyclone Best-Tracks, 1945–2000. Report No. NRL/MR/7540-02-16. <https://www.metoc.navy.mil/jtvc/products/best-tracks/tc-tb-report.html> (2002).
- Moon, I. J. & Kwon, S. J. Impact of upper-ocean thermal structure on the intensity of Korean peninsular landfall typhoons. *Prog. Oceanogr.* **105**, 61–66 (2012).
- Lee, J. H., Pang, I. C. & Moon, J. H. Contribution of the Yellow Sea bottom cold water to the abnormal cooling of sea surface temperature in the summer of 2011. *J. Geophys. Res. Oceans* **121**, 3777–3789 (2016).
- Park, J. H. et al. Rapid decay of slowly moving typhoon Soulik (2018) due to interactions with the strongly stratified Northern East China Sea. *Geophys. Res. Lett.* **46**, 14595–14603 (2019).
- Liu, L., Wang, Y. Q., Zhan, R. F., Xu, J. & Duan, Y. H. Increasing destructive potential of landfalling tropical cyclones over China. *J. Clim.* **33**, 3731–3743 (2020).
- Guan, S. D. et al. Tropical cyclone-induced sea surface cooling over the Yellow Sea and Bohai Sea in the 2019 Pacific typhoon season. *J. Mar. Syst.* **217**, 103509 (2021).
- Balaguru, K. et al. Dynamic potential intensity: an improved representation of the ocean's impact on tropical cyclones. *Geophys. Res. Lett.* **42**, 6739–6746 (2015).
- Cione, J. J. & Uhlhorn, E. W. Sea surface temperature variability in hurricanes: Implications with respect to intensity change. *Mon. Weather Rev.* **131**, 1783–1796 (2003).
- Emanuel, K., DesAutels, C., Holloway, C. & Korty, R. Environmental control of tropical cyclone intensity. *J. Atmos. Sci.* **61**, 843–858 (2004).
- Emanuel, K. A. Thermodynamic control of hurricane intensity. *Nature* **401**, 665–669 (1999).
- Jaimes, B., Shay, L. K. & Uhlhorn, E. W. Enthalpy and momentum fluxes during Hurricane Earl relative to underlying ocean features. *Mon. Weather Rev.* **143**, 111–131 (2015).
- Lin, I. I., Pun, I. F. & Lien, C. C. “Category-6” supertyphoon Haiyan in global warming hiatus: contribution from subsurface ocean warming. *Geophys. Res. Lett.* **41**, 8547–8553 (2014).
- Lin, I. I., Pun, I. F. & Wu, C. C. Upper-ocean thermal structure and the Western North Pacific category 5 typhoons. Part II: dependence on translation speed. *Mon. Weather Rev.* **137**, 3744–3757 (2009).
- Lin, I. I. et al. A tale of two rapidly intensifying supertyphoons Hagibis (2019) and Haiyan (2013). *Bull. Am. Meteor. Soc.* **102**, E1645–E1664 (2021).
- Lin, I. I. et al. The interaction of supertyphoon Maemi (2003) with a warm ocean eddy. *Mon. Weather Rev.* **133**, 2635–2649 (2005).
- Lin, I. I., Wu, C. C., Pun, I. F. & Ko, D. S. Upper-ocean thermal structure and the western North Pacific category 5 typhoons. Part I: ocean features and the category 5 typhoons' intensification. *Mon. Weather Rev.* **136**, 3288–3306 (2008).
- Pun, I. F., Knaff, J. A. & Sampson, C. R. Uncertainty of tropical cyclone wind radii on sea surface temperature cooling. *J. Geophys. Res. Atmos.* **126**, e2021JD034857 (2021).
- Pun, I. F., Lin, I. I., Lien, C. C. & Wu, C. C. Influence of the size of supertyphoon Megi (2010) on SST cooling. *Mon. Weather Rev.* **146**, 661–677 (2018).
- Shay, L. K., Goni, G. J. & Black, P. G. Effects of a warm oceanic feature on Hurricane Opal. *Mon. Weather Rev.* **128**, 1366–1383 (2000).
- Wu, C. C., Tu, W. T., Pun, I. F., Lin, I. I. & Peng, M. S. Tropical cyclone-ocean interaction in Typhoon Megi (2010)A synergy study based on ITOP observations and atmosphere-ocean coupled model simulations. *J. Geophys. Res. Atmos.* **121**, 153–167 (2016).
- Lin, I. I. et al. An ocean coupling potential intensity index for tropical cyclones. *Geophys. Res. Lett.* **40**, 1878–1882 (2013).
- Potter, H., DiMareo, S. F. & Knap, A. H. Tropical cyclone heat potential and the rapid intensification of Hurricane Harvey in the Texas bight. *J. Geophys. Res. Oceans* **124**, 2440–2451 (2019).
- Pun, I. F. et al. Rapid intensification of typhoon Hato (2017) over shallow water. *Sustainability* **11**, 3709 (2019).
- Jacob, S. D., Shay, L. K., Mariano, A. J. & Black, P. G. The 3D oceanic mixed layer response to Hurricane Gilbert. *J. Phys. Oceanogr.* **30**, 1407–1429 (2000).
- Price, J. F. Upper ocean response to a Hurricane. *J. Phys. Oceanogr.* **11**, 153–175 (1981).
- Price, J. F. Metrics of hurricane-ocean interaction: vertically-integrated or vertically-averaged ocean temperature? *Ocean Sci.* **5**, 351–368 (2009).
- Price, J. F., Weller, R. A. & Pinkel, R. Diurnal cycling: observations and models of the upper ocean response to diurnal heating, cooling, and wind mixing. *J. Geophys. Res. Oceans* **91**, 8411–8427 (1986).
- Yang, Y. J. et al. The role of enhanced velocity shears in rapid ocean cooling during Super Typhoon Neptak 2016. *Nat. Commun.* **10**, 1627 (2019).
- Zhang, H., He, H. L., Zhang, W. Z. & Tian, D. Upper ocean response to tropical cyclones: a review. *Geosci. Lett.* **8**, 1–12 (2021).
- D'Asaro, E. A. et al. Impact of typhoons on the ocean in the Pacific. *Bull. Am. Meteor. Soc.* **95**, 1405–1418 (2014).
- Price, J. F., Sanford, T. B. & Forristall, G. Z. Forced stage response to a moving Hurricane. *J. Phys. Oceanogr.* **24**, 233–260 (1994).
- Price, J. F. Internal wave wake of a moving storm. Part I. Scales, energy budget and observations. *J. Phys. Oceanogr.* **13**, 949–965 (1983).
- Glenn, S. M. et al. Stratified coastal ocean interactions with tropical cyclones. *Nat. Commun.* **7**, 10887 (2016).
- Seroka, G. et al. Hurricane Irene sensitivity to stratified coastal ocean cooling. *Mon. Weather Rev.* **144**, 3507–3530 (2016).
- Elzahaby, Y. & Schaeffer, A. Observational insight into the subsurface anomalies of marine heatwaves. *Front. Mar. Sci.* **6**, 745 (2019).
- Hobday, A. J. et al. A hierarchical approach to defining marine heatwaves. *Prog. Oceanogr.* **141**, 227–238 (2016).
- Sen Gupta, A. et al. Drivers and impacts of the most extreme marine heatwaves events. *Sci. Rep.* **10**, 19359 (2020).
- Smith, K. E. et al. Socioeconomic impacts of marine heatwaves: global issues and opportunities. *Science* **374**, 419– (2021).
- Dzwonkowski, B. et al. Compounding impact of severe weather events fuels marine heatwave in the coastal ocean. *Nat. Commun.* **11**, 4623 (2020).
- Ha, K. J. et al. Observations utilizing Korea ocean research stations and their applications for process studies. *Bull. Am. Meteor. Soc.* **100**, 2061–2075 (2019).

41. Huang, H. C. et al. Air-sea fluxes for Hurricane Patricia (2015): comparison with super typhoon Haiyan (2013) and under different ENSO conditions. *J. Geophys. Res. Oceans* **122**, 6076–6089 (2017).
42. Huang, P., Lin, I. I., Chou, C. & Huang, R. H. Change in ocean subsurface environment to suppress tropical cyclone intensification under global warming. *Nat. Commun.* **6**, 7188 (2015).
43. Cione, J. J., Kalina, E. A., Zhang, J. A. & Uhlhorn, E. W. Observations of air-sea interaction and intensity change in Hurricanes. *Mon. Weather Rev.* **141**, 2368–2382 (2013).
44. Emanuel, K. A. The dependence of hurricane intensity on climate. *Nature* **326**, 483–485 (1987).
45. Park, T. et al. Effects of the Changjiang river discharge on sea surface warming in the Yellow and East China Seas in summer. *Cont. Shelf Res.* **31**, 15–22 (2011).
46. Hong, J. S. et al. Role of salinity-induced barrier layer in air-sea interaction during the intensification of a typhoon. *Front. Mar. Sci.* **9**, 844003 (2022).
47. Ha, K. J. et al. Dynamics and characteristics of dry and moist heatwaves over East Asia. *npj Clim. Atmos. Sci.* **5**, 49 (2022).
48. Meehl, G. A. & Tebaldi, C. More intense, more frequent, and longer lasting heat waves in the 21st century. *Science* **305**, 994–997 (2004).
49. Perkins, S. E., Alexander, L. V. & Nairn, J. R. Increasing frequency, intensity and duration of observed global heatwaves and warm spells. *Geophys. Res. Lett.* **39**, L20714 (2012).
50. Russo, S., Sillmann, J. & Fischer, E. M. Top ten European heatwaves since 1950 and their occurrence in the coming decades. *Environ. Res. Lett.* **10**, 124003 (2015).
51. Frölicher, T. L., Fischer, E. M. & Gruber, N. Marine heatwaves under global warming. *Nature* **560**, 360–364 (2018).
52. Oliver, E. C. J. et al. Longer and more frequent marine heatwaves over the past century. *Nat. Commun.* **9**, 1–12 (2018).
53. Lok, C. C. F., Chan, J. C. L. & Toumi, R. Tropical cyclones near landfall can induce their own intensification through feedbacks on radiative forcing. *Commun. Earth Environ.* **2**, 184 (2021).
54. Zhang, Z., Wang, Y. Q., Zhang, W. M. & Xu, J. Coastal ocean response and its feedback to typhoon Hato (2017) over the South China Sea: a numerical study. *J. Geophys. Res. Atmos.* **124**, 13731–13749 (2019).
55. Powell, M. D., Vickery, P. J. & Reinhold, T. A. Reduced drag coefficient for high wind speeds in tropical cyclones. *Nature* **422**, 279–283 (2003).
56. Zhang, J. A., Black, P. G., French, J. R. & Drennan, W. M. First direct measurements of enthalpy flux in the hurricane boundary layer: the CBLAST results. *Geophys. Res. Lett.* **35**, L14813 (2008).

ACKNOWLEDGEMENTS

We are grateful to James F. Price for the PWP model and to Yu-Chiao Liang for the comments during the early stage of this work. Thanks also to the three anonymous reviewers for their constructive comments and feedback. I.P. is supported by the National Science and Technology Council, Taiwan (MOST 111-2111-M-008-016 and NSTC 112-2111-M-008-016). I.M. is supported by Korea Institute of Marine Science &

Technology Promotion (KIMST), funded by the Ministry of Oceans and Fisheries (20210607, Establishment of the ocean research station in the jurisdiction zone and convergence research) and Basic Science Research Program through the National Research Foundation of Korea (NRF) funded by the Ministry of Education (2021R1A2C1005287).

AUTHOR CONTRIBUTIONS

I.P. initiated the research, performed the numerical simulations, and conducted the analyses. I.P., H.H., I.M., and I.L. contributed to the discussion, interpretation, and editing. I.M. and J.J. provided the IORS observational data. I.P. wrote the manuscript with input from H.H., I.M., and I.L.

COMPETING INTERESTS

The authors declare no competing interests.

ADDITIONAL INFORMATION

Supplementary information The online version contains supplementary material available at <https://doi.org/10.1038/s41612-023-00449-5>.

Correspondence and requests for materials should be addressed to Iam-Fei Pun.

Reprints and permission information is available at <http://www.nature.com/reprints>

Publisher's note Springer Nature remains neutral with regard to jurisdictional claims in published maps and institutional affiliations.



Open Access This article is licensed under a Creative Commons Attribution 4.0 International License, which permits use, sharing, adaptation, distribution and reproduction in any medium or format, as long as you give appropriate credit to the original author(s) and the source, provide a link to the Creative Commons license, and indicate if changes were made. The images or other third party material in this article are included in the article's Creative Commons license, unless indicated otherwise in a credit line to the material. If material is not included in the article's Creative Commons license and your intended use is not permitted by statutory regulation or exceeds the permitted use, you will need to obtain permission directly from the copyright holder. To view a copy of this license, visit <http://creativecommons.org/licenses/by/4.0/>.

© The Author(s) 2023